REGULAR ARTICLE

blood advances

Constitutive Ras signaling and *Ink4a/Arf* inactivation cooperate during the development of B-ALL in mice

Tomasz Sewastianik,[1,2] Meng Jiang,[1,3] Kumar Sukhdeo,[4,5] Sanjay S. Patel,[6] Kathryn Roberts,[7] Yue Kang,[1] Ahmad Alduaij,[8] Peter S. Dennis,[1] Brian Lawney,[9] Ruiyang Liu,[1] Zeyuan Song,[1] Jessie Xiong,[10] Yunyu Zhang,[11] Madeleine E. Lemieux,[12] Geraldine S. Pinkus,[6] Jeremy N. Rich,[4] David M. Weinstock,[11] Charles G. Mullighan,[7] Norman E. Sharpless,[10] and Ruben D. Carrasco[1,6]

[1]Department of Oncologic Pathology, Dana-Farber Cancer Institute, Boston, MA; [2]Department of Experimental Hematology, Institute of Hematology and Transfusion Medicine, Warsaw, Poland; [3]Department of Surgical Oncology, The Fourth Affiliated Hospital of Harbin Medical University, Harbin, China; [4]Department of Stem Cell Biology and Regenerative Medicine, Cleveland Clinic, Cleveland, OH; [5]Department of Pathology, Case Western Reserve University, Cleveland, OH; [6]Department of Pathology, Brigham & Women's Hospital, Boston, MA; [7]Department of Pathology, St. Jude Children's Research Hospital, Memphis, TN; [8]Pathology and Laboratory Medicine Institute, Cleveland Clinic Abu Dhabi, Abu Dhabi, United Arab Emirates; [9]Center for Computational Cancer Biology, Dana-Farber Cancer Institute, Boston, MA; [10]Lineberger Comprehensive Cancer Center, School of Medicine, University of North Carolina, Chapel Hill, NC; [11]Department of Medical Oncology, Dana-Farber Cancer Institute, Boston, MA; and [12]Bioinfo, Plantagenet, ON, Canada

Key Points

- Ras pathway activation cooperates with *Ink4a/Arf* locus deletion in B cells to induce a fully penetrant lymphoma/leukemia phenotype in mice.
- These tumors resemble high-risk subtypes of human B-ALL, providing a convenient and highly reproducible model of refractory B-ALL.

Despite recent advances in treatment, human precursor B-cell acute lymphoblastic leukemia (B-ALL) remains a challenging clinical entity. Recent genome-wide studies have uncovered frequent genetic alterations involving RAS pathway mutations and loss of the *INK4A/ARF* locus, suggesting their important role in the pathogenesis, relapse, and chemotherapy resistance of B-ALL. To better understand the oncogenic mechanisms by which these alterations might promote B-ALL and to develop an in vivo preclinical model of relapsed B-ALL, we engineered mouse strains with induced somatic $Kras^{G12D}$ pathway activation and/or loss of *Ink4a/Arf* during early stages of B-cell development. Although constitutive activation of $Kras^{G12D}$ in B cells induced prominent transcriptional changes that resulted in enhanced proliferation, it was not sufficient by itself to induce development of a high-grade leukemia/lymphoma. Instead, in 40% of mice, these engineered mutations promoted development of a clonal low-grade lymphoproliferative disorder resembling human extranodal marginal-zone lymphoma of mucosa-associated lymphoid tissue or lymphoplasmacytic lymphoma. Interestingly, loss of the *Ink4a/Arf* locus, apart from reducing the number of apoptotic B cells broadly attenuated $Kras^{G12D}$-induced transcriptional signatures. However, combined Kras activation and *Ink4a/Arf* inactivation cooperated functionally to induce a fully penetrant, highly aggressive B-ALL phenotype resembling high-risk subtypes of human B-ALL such as *BCR-ABL* and *CRFL2*-rearranged. Ninety percent of examined murine B-ALL tumors showed loss of the wild-type *Ink4a/Arf* locus without acquisition of highly recurrent cooperating events, underscoring the role of *Ink4a/Arf* in restraining Kras-driven oncogenesis in the lymphoid compartment. These data highlight the importance of functional cooperation between mutated Kras and *Ink4a/Arf* loss on B-ALL.

Introduction

B-cell acute lymphoblastic leukemia (B-ALL) is the most common neoplasm among children.[1] By using current therapy regimens, complete remission is attainable in more than 85% of young patients.

Submitted 7 September 2017; accepted 24 September 2017. DOI 10.1182/bloodadvances.2017012211.

The full-text version of this article contains a data supplement.

However, the prognosis after relapse is poor, and B-ALL remains a significant cause of cancer mortality among this age group.[2] Furthermore, as a result of a worse prognosis and higher relapse rate, B-ALL remains a significant clinical problem in adult patients.[1,3,4] B-ALL is a heterogeneous malignancy of B-cell–committed precursor cells that affects bone marrow (BM) and peripheral blood (PB) and is most commonly characterized by a precursor B-ALL immunophenotype ($CD10^+CD19^+TdT^+$ cyt-IgM^+).[1] Over the years, recurrent cytogenetic abnormalities have been used to classify disease subtypes and study their pathogenesis and clinical features.[5]

On a more positive note, recent advances in molecular biology methodology have uncovered a complex genetic landscape, helped to identify new subtypes of B-ALL, and demonstrated alterations in cellular pathways independent of cytogenetic subclasses.[5-8] Among the numerous recently recognized pathogenetic processes in B-ALL, such as lymphoid development, tumor suppression, cytokine receptor signaling, kinase signaling, and chromatin remodeling,[5] Ras pathway mutations (eg, *KRAS*, *NRAS*, *FLT3*, *PTPN11*, and *NF1*) seem particularly important, inasmuch as they are present in up to 40% of relapsed cases and probably originate in small subclones, already present at diagnosis, that for various reasons are unresponsive to chemotherapy.[9-13] Moreover, the true incidence of activated RAS/MAPK signaling may be underestimated, because it can be induced by chromosomal rearrangements such as *BCR-ABL*,[14,15] *CRLF2*,[16-18] and/or other genomic alterations, including those acquired during relapse. Indeed, genomic analysis of presentation/relapsed B-ALL samples provides strong indication of convergence in WNT and RAS-related MAPK pathways.[19]

Altered expression of tumor suppression and cell-cycle regulation genes such as *TP53* and *CDKN2A/B* are also frequently acquired during relapse of B-ALL.[19-21] *CDKN2A* encodes $p16^{INK4A}$ and $p14^{ARF}$ tumor suppressors in humans ($p16^{Ink4a}$ and $p19^{Arf}$ in mice; hereafter referred to as Ink4a and Arf) that play non-overlapping crucial roles in the regulation of cell-cycle progression.[22,23] Both proteins counteract excessive mitogenic signals to promote cellular senescence. The *INK4A/ARF* locus is most frequently deleted in unfavorable hypodiploid, BCR-ABL, and CRLF2 subtypes of B-ALL.[24,25] Therefore, to comprehensively characterize the functional roles of somatic RAS pathway activation and *INK4A/ARF* alterations in B cells, we generated conditional mutant mice overexpressing constitutively active mutant $Kras^{G12D}$ and/or harboring a knockout of a single *Ink4a/Arf* allele. These animals show that Ink4a/Arf restrains the oncogenic potential of $Kras^{G12D}$ mutation and that concurrent Kras activation and loss of *Ink4a/Arf* in $CD19^+$ B cells results in spontaneous development of an aggressive form of B-ALL.

Materials and methods

Engineered mice

Mouse strains bearing either a mutant *LoxP-STOP-LoxP-*$Kras^{G12D}$ knockin allele ($Kras^{G12D}$), *Ink4a/Arf* with floxed exons 2 and 3 ($Ink4a/Arf^{L}$), or a *CD19*-driven Cre recombinase knockin allele ($CD19^{Cre}$) were crossed to generate experimental cohorts.[26-29] $CD19^{Cre/+}$ animals were used as controls. Genotyping was performed as previously described.[30] Cre-mediated excision of the *Ink4a/Arf* conditional allele was tested by Southern blot analysis of genomic DNA isolated from whole testes or $CD19^+$ splenocytes isolated by using magnetic beads (Miltenyi Biotech). Reverse transcription polymerase chain reaction/restriction fragment length polymorphism analyses were performed with RNA isolated from whole testes or $CD19^+$ splenocytes.[30] Survival analysis was performed by using the Kaplan-Meier method and compared by using the log-rank test. All animal experiments were approved by the Institutional Animal Care and Use Committee of the Dana-Farber Cancer Institute.

Histopathology, immunohistochemistry, TUNEL assay, proliferation assay, and flow cytometry

Mice were euthanized at specified time points or when clinical signs of disease were evident; a full histologic examination was performed on each animal to assess for tumor formation. Histology, immunohistochemistry (IHC), and terminal deoxynucleotidyl transferase (TdT) deoxyuridine triphosphate (dUTP) nick-end labeling (TUNEL) assay were performed as in previous studies.[31] Immunofluorescence was performed on paraffin-embedded tissue with anti-mouse CD19 antibody and 4′,6-diamidino-2-phenylindole (DAPI) nuclear counterstain. Apoptotic cells were detected by using the APO-BrdU TUNEL kit (Invitrogen). For quantification of IHC analysis, 5 representative high-power fields were quantified by using ImageJ software (Fiji distribution).[32,33] Flow cytometry using antibody against B220/CD45R and proliferation assay using tritiated thymidine ([^{3}H]dThd) incorporation into DNA were performed as described.[31] For a detailed list of antibodies, see supplemental Methods. Figures display means from 3 independent replicates; *P* values were calculated by using Welch's *t* test.[34]

Western and Southern blotting

Whole-cell protein extracts prepared from $CD19^+$ splenocytes of 8-week-old mice were immunoblotted by using indicated antibodies as described.[31] For a detailed list of antibodies, see supplemental Methods. Genomic DNA collected via the Puregene kit (Gentra Systems) from lymph nodes (LNs) or lungs was used to analyze the immunoglobulin heavy-chain (*IgH*) gene and the T-cell receptor (*TCR*) gene by Southern blotting as described.[31]

Gene expression analysis, array comparative genomic hybridization, and whole-exome sequencing

Duplicate samples of RNA from $CD19^+$ cells from premalignant 8-week-old mice (GSE69367) and from 10 mouse B-ALL tumors (GSE69368) were hybridized to Affymetrix Gene Chip Mouse Genome 430 2.0 arrays (supplemental Methods).

Array comparative genomic hybridization (aCGH) and whole-exome sequencing (WES) were performed by using genomic DNA isolated as for Southern blotting. For aCGH, DNA was hybridized and analyzed as described previously.[35] For WES, libraries were prepared from 100 ng of DNA by using the SureSelectXT2 kit (Agilent Genomics) according to the manufacturer's protocol; thereafter, concentration and quality were checked using Qubit (Life Technologies), Bioanalyzer (Agilent), and quantitative polymerase chain reaction using KAPA Library Quantification kits (Kapa Biosystems) with a 7900HT thermocycler (Applied Biosystems). Samples were loaded onto paired-end

75-bp high-throughput flow cells (Illumina) at a final concentration of 2 pM, and then were sequenced with NextSeq500 (Illumina). FastQ files (PRJNA397401) were aligned, processed with Mutect2,[36] and filtered to remove remaining germ line variants (supplemental Methods).

Results

$Kras^{G12D}$ mutation and *Ink4a/Arf* loss result in expansion of B cells in young engineered mice

To model the cooperative interactions of 2 concomitant genetic lesions found frequently in relapsed human B-ALL, mouse strains bearing either a mutant $Kras^{G12D}$ knockin allele, a conditional *Ink4a/Arf* knockout allele, or a *CD19*-driven Cre recombinase knockin allele were crossed to generate cohorts of single-mutant $CD19^{Cre/+}Kras^{G12D/+}$ and $CD19^{Cre/+}Ink4a/Arf^{L/+}$ as well as $CD19^{Cre/+}Kras^{G12D/+}Ink4a/Arf^{L/+}$ compound-mutant mice.[26-28] The $CD19^{Cre}$ allele drives Cre recombinase expression during most stages of B-cell development starting with pre-B cells.[26] We confirmed that Cre-mediated deletion of the *Ink4a/Arf* allele and activation of the mutated $Kras^{G12D/+}$ allele were specific and efficient in $CD19^+$ splenic B cells from engineered mice (supplemental Figure 1).

To initially assess the role of $Kras^{G12D}$ and/or loss of *Ink4a/Arf* during B-cell development, we performed physical examination of young $CD19^{Cre/+}Kras^{G12D/+}$, $CD19^{Cre/+}Ink4a/Arf^{L/+}$, and $CD19^{Cre/+}Kras^{G12D/+}Ink4a/Arf^{L/+}$ mice. Significant differences in weight, posture, and overall appearance between young control $CD19^{Cre/+}$ and engineered mice were not observed. Therefore, groups of 3 single- and double-mutant animals were euthanized at 8 weeks of age (ie, preceding disease development) and rigorously assessed for alterations of lymphoid organs and B cells. Pathologic examination revealed significantly enlarged spleens with increased numbers of mononuclear cells in $Kras^{G12D}$-mutated animals with or without *Ink4a/Arf* inactivation (Figure 1A; Table 1), but obvious histologic differences in spleens and LNs between the mutant genotypes and $CD19^{Cre/+}$ controls were not found (Figure 1B; supplemental Figure 2A). IHC analysis for the CD3 and B220 markers revealed normal T- and B-cell ratios (Figure 1B; supplemental Figure 2A). Of note, there was no obvious increase in number of progenitor or blast cells as measured by TdT staining in the BM, spleen, and LNs from young mutant mice compared with $CD19^{Cre/+}$ controls (Figure 1B-C; supplemental Figure 2A-B).

However, in agreement with the gross pathologic examination, an increase was noted by flow cytometry in splenic $B220^+$ B cells of mice with the $Kras^{G12D}$ mutation compared with $CD19^{Cre/+}$ and $CD19^{Cre/+}Ink4a/Arf^{L/+}$ mice (Figure 1D). Likewise, a significant increase in percentage of proliferating ($Ki\text{-}67^+$) cells within spleen B-cell areas of $CD19^{Cre/+}Kras^{G12D/+}$, and $CD19^{Cre/+}Kras^{G12D/+}Ink4a/Arf^{L/+}$ mice was observed in comparison with $CD19^{Cre/+}$ controls and $CD19^{Cre/+}Ink4a/Arf^{L/+}$ mice (Figure 1E). TUNEL staining revealed fewer apoptotic cells within germinal center B-cell areas in $CD19^{Cre/+}Kras^{G12D/+}$, $CD19^{Cre/+}Ink4a/Arf^{L/+}$, and $CD19^{Cre/+}Kras^{G12D/+}Ink4a/Arf^{L/+}$ mice compared with $CD19^{Cre/+}$ controls (Figure 1F). Collectively, these results suggest that the $Kras^{G12D}$ mutation strongly enhances proliferation and reduces apoptosis of B cells, whereas *Ink4a/Arf* loss inhibits B-cell apoptosis and, to a certain degree, reduces $Kras^{G12D}$-induced proliferation in vivo.

$Kras^{G12D}$ mutation induces transcriptional changes that prime cells for hypersensitivity to proliferative stimuli

To elucidate molecular mechanisms responsible for $Kras^{G12D}$ mutation and/or *Ink4a/Arf* inactivation–driven expansion of B cells, we performed microarray gene expression analysis in $CD19^+$ B cells from 8-week-old engineered mice. The most differentially expressed genes (fold change >2; $P < .01$) between control, single-, and double-mutant mice are shown in the heat map (Figure 2A; supplemental Table 1). Next, to identify the biological processes underlying observed phenotypical changes, we performed gene-set enrichment analysis (GSEA) of expression data from mutant compared with control mice. Marked upregulation of gene signatures related to proliferation, Ras-related signaling pathways, apoptosis, rewired cellular metabolism, DNA repair, and pre-B stage of B-cell development were observed in both $CD19^{Cre/+}Kras^{G12D/+}$ and $CD19^{Cre/+}Kras^{G12D/+}Ink4a/Arf^{L/+}$ mice (Figure 2B; supplemental Figure 3A-B). Consistent with our previous observations, the proliferative signature in $CD19^+$ B cells from $CD19^{Cre/+}Ink4a/Arf^{L/+}$ mice was less pronounced; instead, upregulation of several signaling pathways related to independence from external growth signals and retention of stemness was noted (Figure 2B; supplemental Figure 3A,C). Interestingly, *Ink4a/Arf* inactivation suppressed, at least in part, a signature upregulated by Kras signaling.

To validate one of the most compelling transcriptomic findings at the protein level, we examined both cyclin D2 (CCND2) expression and the proliferative potential of $CD19^+$ B cells. Higher cyclin D2 expression in B cells from $CD19^{Cre/+}Kras^{G12D/+}$ and $CD19^{Cre/+}Kras^{G12D/+}Ink4a/Arf^{L/+}$ compared with $CD19^{Cre/+}$ and $CD19^{Cre/+}Ink4a/Arf^{L/+}$ mice was observed by immunoblotting and IHC (Figure 2C-D). Next, isolated $CD19^+$ B cells from the animals' spleens were treated with lipopolysaccharide and assessed for in vitro proliferative potential. Consistently, proliferation was highest in $CD19^+$ B cells with $Kras^{G12D}$ mutation with or without loss of *Ink4a/Arf* (Figure 2E). These results indicate that $Kras^{G12D}$ and *Ink4a/Arf* mutations drive perturbations in B-cell signaling and proliferation and that *Ink4a/Arf* deletion restrains $Kras^{G12D}$-induced changes.

$CD19^{Cre/+}Kras^{G12D/+}$ and $CD19^{Cre/+}Ink4a/Arf^{L/+}$ mice develop distinct subtypes of B-cell leukemia/lymphoma

Given the molecular and functional changes induced by mutant $Kras^{G12D}$ and loss of *Ink4a/Arf*, we evaluated cohorts of $CD19^{Cre/+}Kras^{G12D/+}$ and $CD19^{Cre/+}Ink4a/Arf^{L/+}$ mice over a span of 75 weeks, after which we euthanized any remaining animals and subjected them to thorough pathologic and histologic examination. Notably, during this aging period, 2 of a total of 20 $CD19^{Cre/+}Kras^{G12D/+}$ mice developed weight loss and hunched posture, requiring euthanasia (Figure 3A; Table 1). Upon histologic examination, only minimal distortion of LNs and spleen architecture was noted in both animals. In the lungs, however, a nodular lymphoid infiltrate composed predominantly of small atypical cells was observed (Figure 3B). All other tissues, including the BM and PB, seemed to be unaffected. The atypical lymphoid cells were predominantly composed of $B220^+BCL6^-TdT^-$ B cells with a low proliferative rate as evaluated by Ki-67 immunostaining and were varyingly infiltrated by $CD3^+CD5^+$ T cells and $CD138^+$ plasma

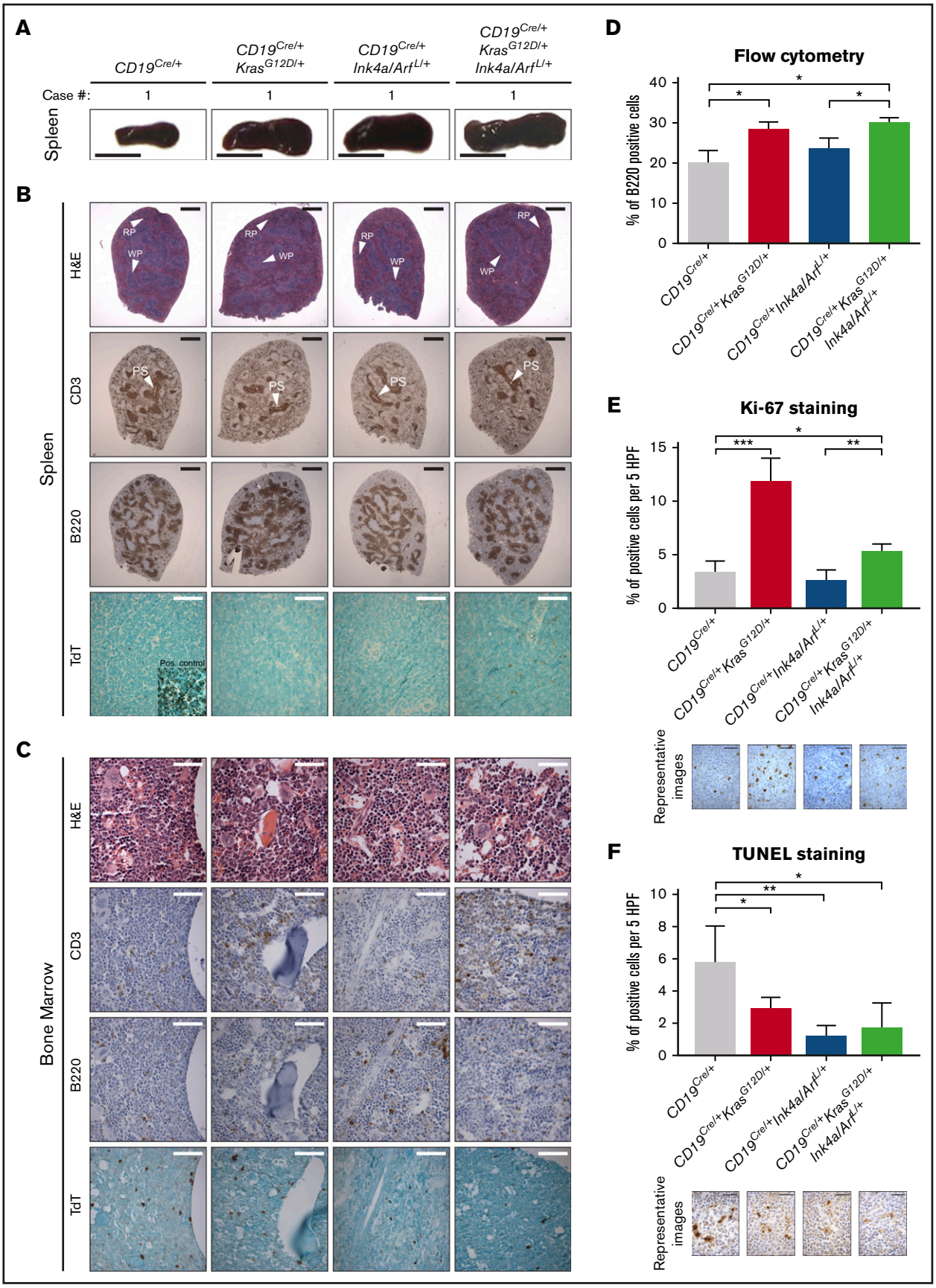
A
CD19Cre/+
CD19Cre/+ KrasG12D/+
CD19Cre/+ Ink4a/ArfL/+
CD19Cre/+ KrasG12D/+ Ink4a/ArfL/+
Case #: 1 1 1 1
Spleen
B
Spleen
H&E
CD3
B220
TdT
RP
WP
PS
Pos. control
C
Bone Marrow
H&E
CD3
B220
TdT
D
Flow cytometry
% of B220 positive cells
0 10 20 30 40
*
*
*
CD19Cre/+
CD19Cre/+ KrasG12D/+
CD19Cre/+ Ink4a/ArfL/+
CD19Cre/+ KrasG12D/+ Ink4a/ArfL/+
E
Ki-67 staining
% of positive cells per 5 HPF
0 5 10 15
***
*
**
Representative images
F
TUNEL staining
% of positive cells per 5 HPF
0 2 4 6 8 10
*
**
*
Representative images

Figure 1.

Table 1. Summary of mouse phenotypes

	$CD19^{Cre/+}$	$CD19^{Cre/+}Kras^{G12D/+}$	$CD19^{Cre/+}Ink4a/Arf^{L/+}$	$CD19^{Cre/+}Kras^{G12D/+}Ink4a/Arf^{L/+}$
Premalignant				
Number of mice	3	3	3	3
Spleen weight, mg	127 ± 12	194 ± 6**	173 ± 12**	213 ± 6**†*
Spleen cells × 10^7	10.6 ± 0.6	14.0 ± 0.8**	12.6 ± 1.2 (ns)	16.5 ± 1.0**†*
Malignant				
No. of mice	10	20	20	26
Lymphoma type	None (10 of 10)	Low-grade B lymphoma (8 of 20)	Pre-B-ALL (12 of 20)	Pre-B-ALL (26 of 26)

Engineered mice of the indicated genotypes were analyzed before overt malignancy (premalignant; 8 weeks of age) or following development of leukemia/lymphoma (malignant). For spleen weight and cell number, the standard deviation is provided.

ns, not significant.

P values were calculated relative to $CD19^{Cre/+}$ or $CD19^{Cre/+}Ink4a/Arf^{L/+}$ (†) using Welch's *t* test. *$P \leq .05$; **$P \leq .01$.

cells (Figure 3B). Southern blot analysis of the *IgH* gene locus showed a minor clonal band in relation to the corresponding band in the germ line (no clonal bands were observed for the *TCR* locus; Figure 3C), a finding consistent with a clonal low-grade B-cell lymphoproliferative disorder such as extranodal marginal zone lymphoma of mucosa-associated lymphoid tissue or lymphoplasmacytic lymphoma in humans.[1] This phenotype was likewise noted in 6 of the 18 $CD19^{Cre/+}Kras^{G12D/+}$ mice that seemed to be disease free at 75 weeks (supplemental Figure 4). Moreover, WES analysis (supplemental Figure 6D) revealed the lack of any highly recurrent secondary loss-of-function or missense mutations in 6 analyzed lymphomas, underscoring the important role of Kras mutation in initiating this low-grade B-cell malignancy. All 10 of the $CD19^{Cre/+}$ controls lacked this phenotype and were histologically unremarkable (Figure 3A; supplemental Figure 4).

During the same 75-week period, 4 of 20 $CD19^{Cre/+}Ink4a/Arf^{L/+}$ mice developed more aggressive disease characterized by weight loss, hunched posture, and lymphadenopathy (Figure 3A; Table 1). Enlarged LNs and splenomegaly were observed at necropsy in all affected mice (Figure 3D). Histologic examination revealed massive distortion of LNs and spleen evidenced by a diffuse monotonous population of blasts (Figure 3E; supplemental Figure 5). A starry-sky pattern with frequent tingible body macrophages and mitotic figures was observed (Figure 3E). Atypical cells were predominantly of the $B220^+CD19^+TdT^+CD3^-CD5^-CD10^+$cyt-$IgM^+$ phenotype and had a very high proliferation rate according to Ki-67 immunostaining (Figure 3E), all of which were consistent with a high-grade B-cell lymphoproliferative disorder such as precursor B-ALL.[1] The atypical lymphoid cells diffusely infiltrated other organs, including the BM, PB, liver, skin, lungs, intestine, and peridural space (Figure 3E; supplemental Figure 5; data not shown). Clonal bands for the *IgH* gene were detected (Figure 3F). Precursor B-ALL was also observed in 8 of the remaining 16 $CD19^{Cre/+}Ink4a/Arf^{L/+}$ mice that seemed to be disease free according to visual examination at 75 weeks of age, but whose disease was evident at necropsy (supplemental Figure 5). In sum, although $Kras^{G12D}$ mutation induced significant transcriptional and functional changes in B cells, it gave rise to only a low-grade mature B-cell malignancy in our model, in contrast with *Ink4a/Arf* loss, which drives the high-grade immature B-cell malignant phenotype.

Kras activation and *Ink4a/Arf* loss cooperate in B-ALL development

In contrast to the relatively low penetrance and long latency observed in single-mutant mice, significantly faster tumor development and higher penetrance were seen in $CD19^{Cre/+}Kras^{G12D/+}Ink4a/Arf^{L/+}$ animals, with each of 26 mice developing cancer within 75 weeks (Figure 3A; Table 1). Animals seemed ill with hunched posture, weight loss, anemia, hind-limb paralysis, and adenopathy (Figure 4A). Massively enlarged LNs and spleens, in addition to pale long bones of the legs and white nodules in the livers and spleens, were observed at necropsy (Figure 4A; data not shown). Histologic examination revealed that most tissues were infiltrated with $B220^+CD19^+TdT^+CD3^-CD5^-CD10^+$ lymphoblasts with a proliferative index similar to that seen in $CD19^{Cre/+}Ink4a/Arf^{L/+}$ mice (Figure 4B; supplemental Figure 5). One or 2 major bands for the *IgH* gene, but not for the *TCR* gene, were detected in most samples by Southern blot analysis, indicating that they were monoclonal or biclonal B-cell neoplasms with immunophenotypes of precursor B-ALL (Figure 4C).

Figure 1. Analysis of 8-week-old mice with conditional expression of $Kras^{G12D}$ and loss of *Ink4a/Arf*. (A) Representative gross pictures of dissected spleens from mice of the indicated genotypes. Scale bar, 1 cm. (B-C) Representative histologic and IHC analyses of CD3, B220, and TdT expression in (B) spleens and (C) BM from mice of the indicated genotypes. Inset, positive control: TdT staining of thymus from the same mouse. Scale bars: black, 1 mm; white, 50 μm (see supplemental Figure 2). (D) Mean percentage of $B220^+$ cells assessed by flow cytometry in splenocytes from mice of the indicated genotype; error bars represent ± standard deviation (SD) of 3 different mice per genotype. *P* values were calculated by using Welch's *t* test. (E-F) Differences in the number of proliferating and apoptotic cells assessed by Ki-67 (E) IHC analysis of B-cell areas and (F) TUNEL assay of germinal center areas, respectively, in spleens from mice of the indicated genotypes, calculated using ImageJ. Bar plots represent mean number of cells per 5 high-power fields (HPFs); error bars ± SD. *P* values were calculated by using Welch's *t* test. Representative images are shown below the graphs. Scale bar, 25 μm. Two independent assays were performed for all experiments for which statistics were calculated. *$P \leq .05$, **$P \leq .01$, ***$P \leq .001$. H&E, hematoxylin and eosin; PS, periarterial sheath; RP, red pulp; WP, white pulp.

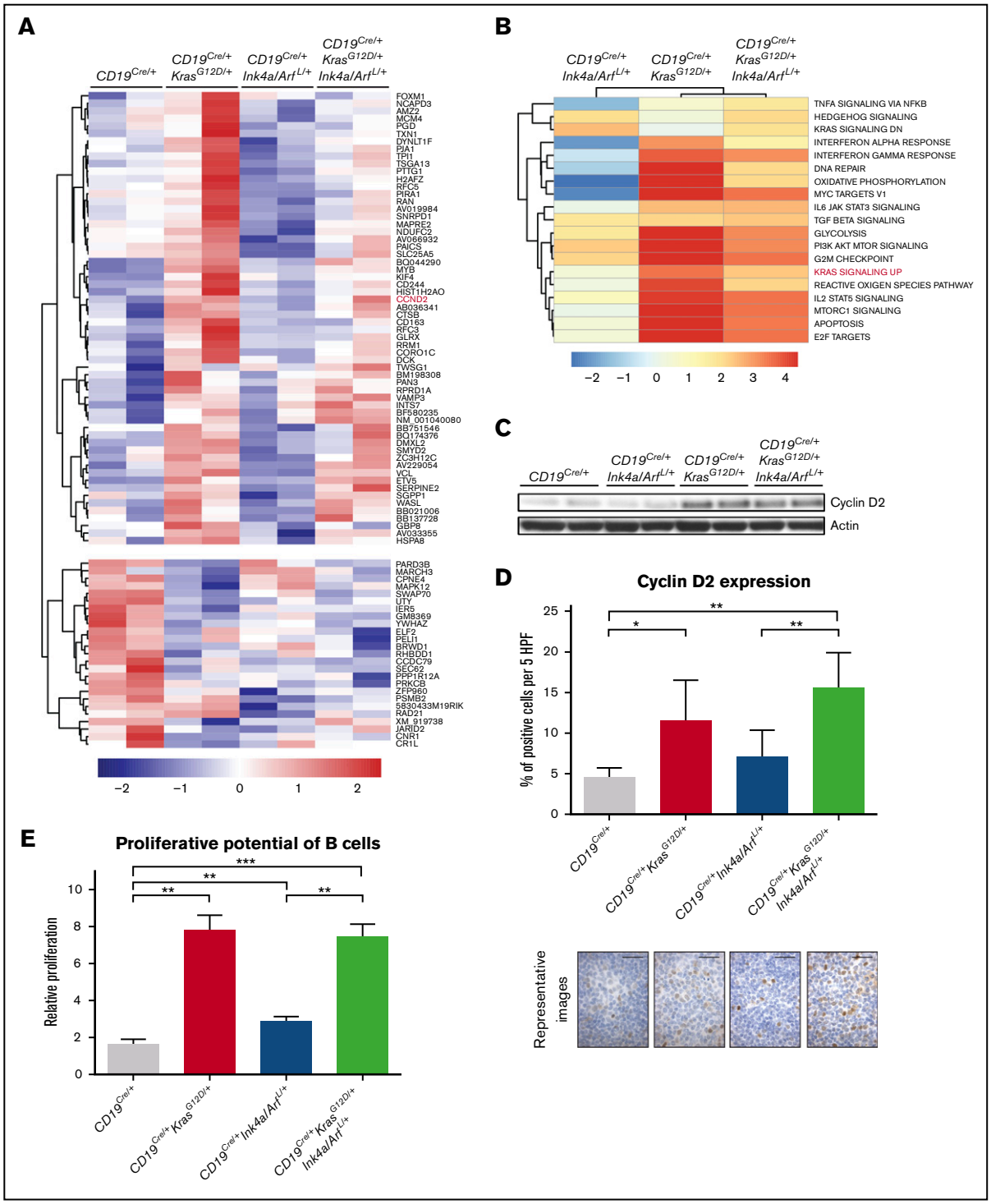

Figure 2. Gene expression analysis of CD19$^+$ B cells from 8-week-old engineered mice. (A) Heat map of the most distinctive sets of differentially expressed genes across indicated genotypes. Values are row-normalized. Cyclin D2 (CCND2) is highlighted in red and validated in panels C and D (see supplemental Table 1). (B) Summary of changes in biological processes and pathways measured by GSEA in CD19$^+$ B cells from mice of indicated genotypes compared with *CD19*$^{Cre/+}$ control mice. Color scale represents −log10 false discovery rate (FDR) from GSEA; positive sign reflects correlation to mutant genotype, negative sign reflects correlation to *CD19*$^{Cre/+}$ control (see supplemental Figure 3). (C-D) Cyclin D2 expression evaluated by (C) immunoblotting in CD19$^+$ B cells and (D) IHC in the B-cell areas of spleens from mice of the indicated genotypes, calculated by using ImageJ. Bar plots present mean percentage of cells per 5 high-power fields; error bars ± SD. *P* values were calculated by using Welch's *t* test. Representative images are shown below the graphs. Scale bar, 25 μm. (E) Impact of Kras^{G12D} mutation and *Ink4a/Arf* loss on proliferative potential of CD19$^+$ B cells from mice of the indicated genotype, evaluated by tritiated thymidine ([^{3}H]dThd) incorporation. CD19$^+$ B cells were isolated, stimulated with lipopolysaccharide (20 μg/mL) for 48 hours, and pulsed with [^{3}H]dThd for the final 16 hours of growth. Incorporated [^{3}H]dThd was measured by scintillation counting. Bars represent mean and error bars ± SD of triplicate cultures. *P* values were calculated by using Welch's *t* test. Two independent assays were performed for all experiments for which statistics were calculated. *$P \leq .05$, **$P \leq .01$, ***$P \leq .001$.

Oncogenic Ras signaling is constrained in some tissue types by Ink4a/Arf tumor suppressors.[23,30,37] Therefore, we suspected that selective pressure might cause loss of heterozygosity (LOH) at the wild-type (WT) *Ink4a/Arf* locus during B-ALL development. Southern blot analysis of this locus revealed preservation of the WT allele in every low-grade B-cell lymphoma in the *CD19*$^{Cre/+}$*Kras*^{G12D} mice; however, 4 of 8 precursor B-ALL tumors in *CD19*$^{Cre/+}$*Ink4a/Arf*$^{L/+}$ mice showed only a faint WT band indicative of LOH (Figure 5A). The residual faint band is most likely the result of contaminating WT hematopoietic and/or stromal cells as evidenced by positive anti-Arf immunostaining (Figure 5B). Moreover, 9 of 10 *CD19*$^{Cre/+}$*Kras*$^{G12D/+}$*Ink4a/Arf*$^{L/+}$ precursor B-ALL tumors had *Ink4a/Arf* LOH (Figure 5A). Given these intriguing results, we generated a small (n = 4) cohort of *CD19*$^{Cre/+}$*Kras*$^{G12D/+}$*Ink4a/Arf*$^{L/L}$ mice with homozygous inactivation of *Ink4a/Arf* and found that these animals succumbed within the first 20 weeks of life with a rapidly progressive form of pre-B-ALL (Figure 5C). Collectively, these data indicate that activated Ras signaling promotes the pathogenesis of the pre-B-ALL, but is restricted by *Ink4a/Arf* tumor suppressor control of the cell cycle, and that simultaneous Kras activation and *Ink4a/Arf* loss cooperate during precursor B-ALL development.

The next issue that had to be addressed was whether Kras^{G12D} mutation and *Ink4a/Arf* inactivation are sufficient to promote leukemogenesis, or whether other cooperating genetic lesions are required. Accordingly, aCGH and WES were performed on tumors from 10 *CD19*$^{Cre/+}$*Kras*$^{G12D/+}$*Ink4a/Arf*$^{L/+}$ mice to analyze them for secondary chromosomal copy number variations and mutations (supplemental Figure 6A-D). No highly recurrent secondary loss-of-function or missense mutations were identified; however, several common copy number variations were observed among 10 tumors in our engineered mice. One of the most recurrent alterations (60%) was gain of chromosome 15 (harboring the *Myc* oncogene)[38]; therefore, it cannot be excluded that other cooperative lesions in the genome might accelerate the onset of leukemia. Nevertheless, it was found that lymphoblasts from *CD19*$^{Cre/+}$*Kras*$^{G12D/+}$*Ink4a/Arf*$^{L/+}$ mice lacked morphologic features typically associated with *Myc* gene translocation[1] and did not exhibit increased overexpression of Myc protein (supplemental Figure 6C). Moreover, the transcriptional signatures of our murine B-ALL tumors strongly resembled those of B cells from young *CD19*$^{Cre/+}$*Kras*$^{G12D/+}$*Ink4a/Arf*$^{L/+}$ mice (supplemental Figure 7; supplemental Table 1), suggesting that Kras^{G12D} mutation and *Ink4a/Arf* loss profoundly influenced transcriptional profiles in our pre-B-ALL model. Taken together, the data supported the hypothesis that loss of the functional allele at the *Ink4a/Arf* locus is rate-limiting in precursor B-ALL tumorigenesis and is accelerated by oncogenic Ras signaling in this model.

B-ALL tumors arising in *CD19*$^{Cre/+}$*Kras*$^{G12D/+}$*Ink4a/Arf*$^{L/+}$ mice most closely resemble human BCR-ABL subtype

Immunohistochemical characterization of B-ALL tumors in *CD19*$^{Cre/+}$*Kras*$^{G12D/+}$*Ink4a/Arf*$^{L/+}$ mice indicated that the cells were arrested at early stages of development. To further evaluate this finding, gene expression profiling was performed in 10 randomly selected *CD19*$^{Cre/+}$*Kras*$^{G12D/+}$*Ink4a/Arf*$^{L/+}$ B-ALL tumors. The resulting transcriptional profiles were then compared with a reference data set from normal mouse lymphocyte populations that included purified pro-B, pre-B, immature B, and mature B cells.[39] Unsupervised hierarchical clustering analysis demonstrated that 9 of 10 *CD19*$^{Cre/+}$*Kras*$^{G12D/+}$*Ink4a/Arf*$^{L/+}$ B-ALL tumors were most similar to normal pre-B cells, with the tenth one more closely resembling normal pro-B cells than immature or mature B cells (Figure 6A). The findings were consistent with the pattern of Cre expression in CD19$^{Cre/+}$ mice[26] as well as with the gene expression profile of premalignant CD19^{+} B cells from *CD19*$^{Cre/+}$*Kras*$^{G12D/+}$*Ink4a/Arf*$^{L/+}$ mice (supplemental Figure 3B) and suggest that Kras^{G12D} mutation together with *Ink4a/Arf* deletion arrests B-cell development at the pre-B-cell stage during neoplastic transformation.

The utility of genetically engineered mouse models of cancer can sometimes be limited by clinico-pathologic incongruence with their human counterparts. It was surmised, however, that the cellular characteristics and aggressive phenotype of B-ALL in *CD19*$^{Cre/+}$*Kras*$^{G12D/+}$*Ink4a/Arf*$^{L/+}$ mice would resemble a poor-prognosis form of human B-ALL. To investigate this possibility, the most differentially expressed genes in murine *CD19*$^{Cre/+}$*Kras*$^{G12D/+}$*Ink4a/Arf*$^{L/+}$ B-ALL were identified and compared with normal mouse pre-B cells.[39] Next, the enrichment of our tumor signature was assessed by GSEA, along with other hallmark signatures in human B-ALL, classified according to BCR-ABL, hyperdiploid, TEL-AML, TCF3-PBX1, and MLL subgroups.[40,41] Genes upregulated in *CD19*$^{Cre/+}$*Kras*$^{G12D/+}$*Ink4a/Arf*$^{L/+}$ B-ALL (labeled "tumor vs Pre-B up") as well as the hallmark Kras (up- but not downregulated) and other signaling signatures were most significantly enriched in the BCR-ABL subtype of human B-ALL (Figure 6B; supplemental Figure 7), which has historically been associated with poor outcome.[42] The gene-set profiles of the hyperdiploid human B-ALL also correlated with the murine tumor signature, although to a lesser degree and without any enrichment of the Kras signatures.

To minimize the possibility that the resemblance of our mouse model to human leukemia results from the convergence of Ras-activated signaling pathways with pro-proliferative activated kinase and/or cytokine receptor signals associated with *BCR-ABL1* Philadephia chromosome–like (Ph-like) as well as *CRLF2* alterations, GSEA was next performed in human B-ALL tumors with known RAS mutational status,[43,44] and in relation to the Ph-like and CRLF2 subtypes. Importantly, significant upregulation of the *CD19*$^{Cre/+}$*Kras*$^{G12D/+}$*Ink4a/Arf*$^{L/+}$ B-ALL transcriptional signature was observed in leukemic blasts with RAS mutations compared with WT RAS from all B-ALL patients (Figure 6C; all_RAS, black box) regardless of Ph-like expression profile (Figure 6C; no_Ph_like, black box). Moreover, the murine tumor signature was most highly enriched in human blasts with *CRLF2* rearrangements but lacking the Ph-like signature compared with other categories and with RAS mutations compared with WT RAS (Figure 6C; CRLF2_non_Ph_like, black box). It is worth mentioning that *CRLF2* rearrangements are also associated with poor clinical outcome.[16] The cross-species analyses consistently demonstrated that B-ALL tumors in the *CD19*$^{Cre/+}$*Kras*$^{G12D/+}$*Ink4a/Arf*$^{L/+}$ mice recapitulate gene expression programs in poor-prognosis subgroups of human B-ALL that harbor *BCR-ABL* and *CRLF2* rearrangements. Furthermore, these observations suggest that RAS mutations have a high impact on B-ALL blast transcriptional profiles and that our engineered mouse models, at least to a certain degree, recapitulate the alterations observed in human B-ALL.

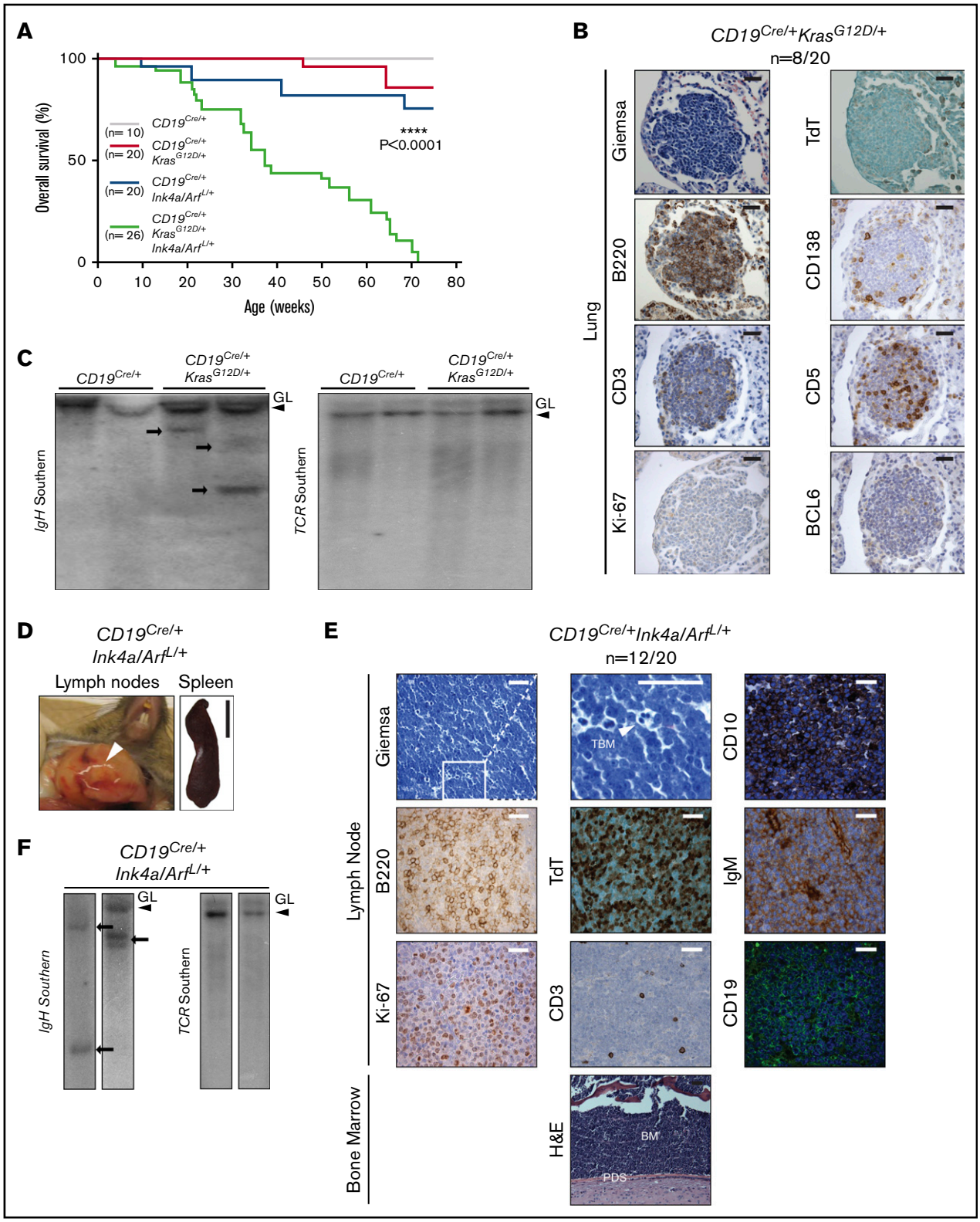

Figure 3. Development of a clonal low-grade B-cell lymphoma and pre-B-ALL in engineered mice. (A) Kaplan-Meier survival plots illustrating overall survival of mouse cohorts according to genotype. *P* values were calculated by using the log-rank test. (B) Histologic and IHC stains of indicated markers in a representative example of low-grade B-cell lymphoma involving the lungs of a *CD19*$^{Cre/+}$*Kras*$^{G12D/+}$ mouse. Scale bar, 25 μm (see supplemental Figure 4). (C) Southern blot analysis for the immunoglobulin heavy chain (*IgH*) (left) and T-cell receptor (*TCR*) (right) genes in the same genomic DNA isolated from *CD19*$^{Cre/+}$ LNs and *CD19*$^{Cre/+}$*Kras*$^{G12D/+}$ lymphomas. Clonal bands are present for the *IgH* gene (arrows) but not for *TCR* (see supplemental Figure 6D). (D) Representative gross pictures of enlarged LNs (white arrow) and

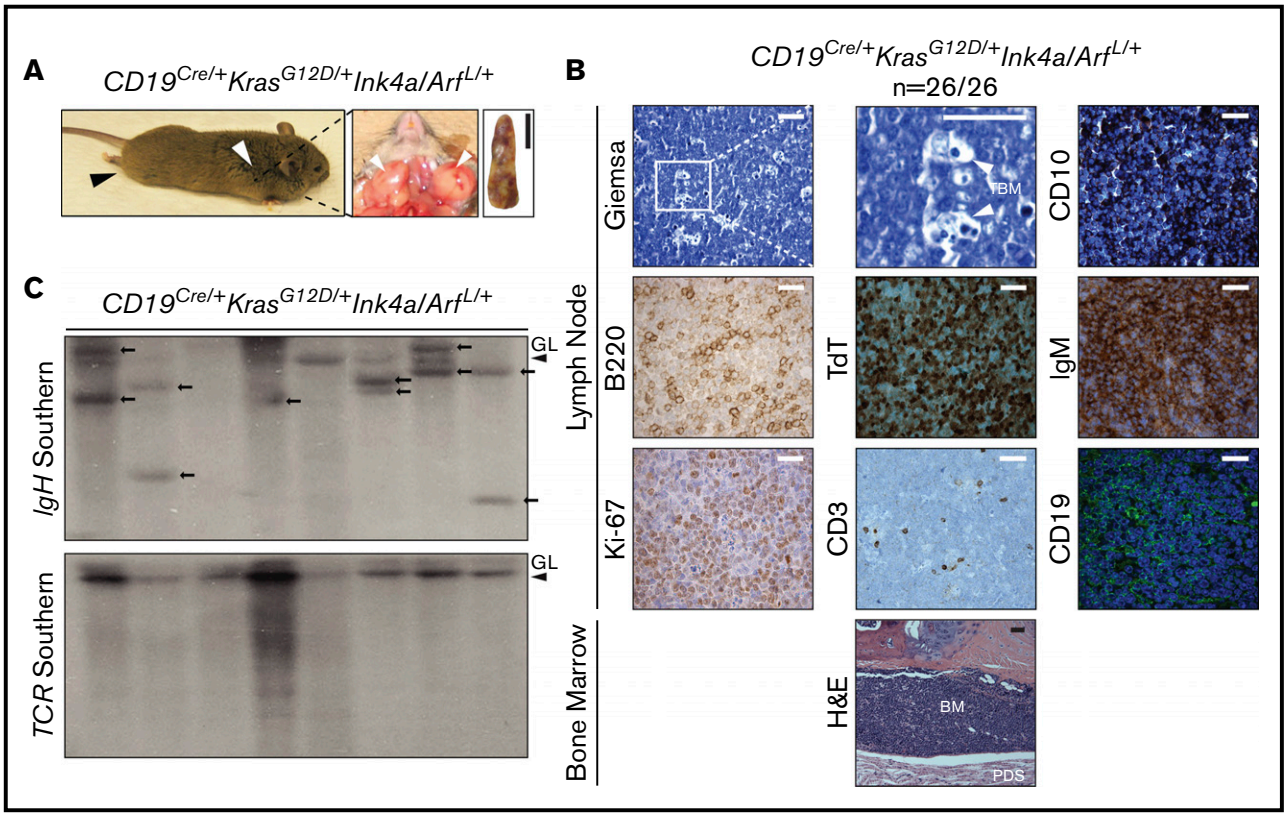

Figure 4. Development of a fully penetrant, highly aggressive B-ALL in Kras$^{G12D/+}$ and *Ink4a/Arf* double-mutant mice. (A) Representative images of enlarged LNs (middle, white arrows) and spleen (right) from a *CD19*$^{Cre/+}$*Kras*$^{G12D/+}$*Ink4a/Arf*$^{L/+}$ mouse with pre-B-ALL. Representative whole-body photograph of *CD19*$^{Cre/+}$*Kras*$^{G12D/+}$ *Ink4a/Arf*$^{L/+}$ mouse with pre-B-ALL (left). White arrow denotes cervical lymphadenopathy; black arrow denotes lagging hind-limb paralysis due to peridural space involvement. Scale bar, 1 cm. (B) Histologic, IHC, and immunofluorescent stains of indicated markers in LN and BM from a representative *CD19*$^{Cre/+}$*Kras*$^{G12D/+}$*Ink4a/Arf*$^{L/+}$ mouse with B-ALL. CD19 staining is shown in green with blue DAPI nuclear counterstain. Note cytoplasmic expression of IgM in B-ALL cells and infiltration of B-ALL cells in the BM and peridural space (PDS) contributing to paralysis (bottom H&E). Scale bars: white, 25 μm; black, 50 μm (see supplemental Figure 5). (C) Southern blot analysis for *IgH* (left) and *TCR* (right) genes in the same genomic DNA isolated from *CD19*$^{Cre/+}$*Kras*$^{G12D/+}$*Ink4a/Arf*$^{L/+}$ leukemias. Clonal bands are present for the *IgH* gene (arrows) but not for *TCR*. Absence of GL band in some tumor DNA samples indicates almost complete replacement with lymphoma cells.

Discussion

In this study, we demonstrate that somatic activation of 1 *Kras*$^{G12D/+}$ allele and concurrent heterozygous deletion of *Ink4a/Arf* during early stages of B-cell development alter transcriptional profiles of CD19^{+} B cells and result in enhanced proliferation and decreased apoptosis. As a consequence, 40% of *CD19*$^{Cre/+}$*Kras*$^{G12D/+}$ mice developed a clonal low-grade B-cell lymphoproliferative disorder, whereas 60% of *CD19*$^{Cre/+}$*Ink4a/Arf*$^{L/+}$ mice developed a more aggressive precursor B-ALL phenotype. Concurrent Kras$^{G12D/+}$ mutation and *Ink4a/Arf* deletion in CD19^{+} B cells cooperatively induced a fully penetrant, highly aggressive B-ALL phenotype that resembled BCR-ABL and CRLF2 subtypes of human B-ALL.

The high prevalence of activating RAS pathway mutations (~35%), either direct or through other means such as *BCR-ABL* and *CRLF2* chromosomal translocations in newly diagnosed and relapsed cases of human B-ALL indicates its importance in the pathogenesis of this form of leukemia.[9,11-19,45] However, the exact role of RAS activation in B-ALL is still debatable. Previous studies show that RAS mutations can be initiating as well as secondary events.[9] Our findings presented in this article demonstrate that, although Ras activation as the initiating event may not be sufficient by itself to induce high-grade leukemia/lymphoma, it can in fact induce dramatic transcriptional changes that prime cells to become hypersensitive to proliferative stimuli, as well as leading to the development of clonal low-grade B-cell lymphoproliferative disorder. However, because Kras mutations have not been reported in human MALT and LPL,[46,47] the possible role of such mutations in the development of these types of low-grade B-cell lymphoproliferative disorders needs to be further investigated.

Figure 3. (continued) spleen from *CD19*$^{Cre/+}$*Ink4a/Arf*$^{L/+}$ mouse with pre-B-ALL. Scale bar, 1 cm. (E) Histologic, IHC, and immunofluorescent stains of indicated markers in LNs and BM from representative *CD19*$^{Cre/+}$*Ink4a/Arf*$^{L/+}$ mouse with B-ALL. CD19 staining shown in green with blue 4′,6-diamidino-2-phenylindole (DAPI) nuclear counterstain. Note cytoplasmic expression of IgM in B-ALL cells. TBG, tingible body macrophage. Scale bars: white, 25 μm; black, 50 μm (see supplemental Figure 5). (F) Southern blot analysis for the *IgH* (left) and *TCR* (right) genes in the same genomic DNA isolated from *CD19*$^{Cre/+}$*Ink4a/Arf*$^{L/+}$ leukemias. Clonal bands are present for the *IgH* gene (arrows) but not for *TCR*. GL, germ line band.

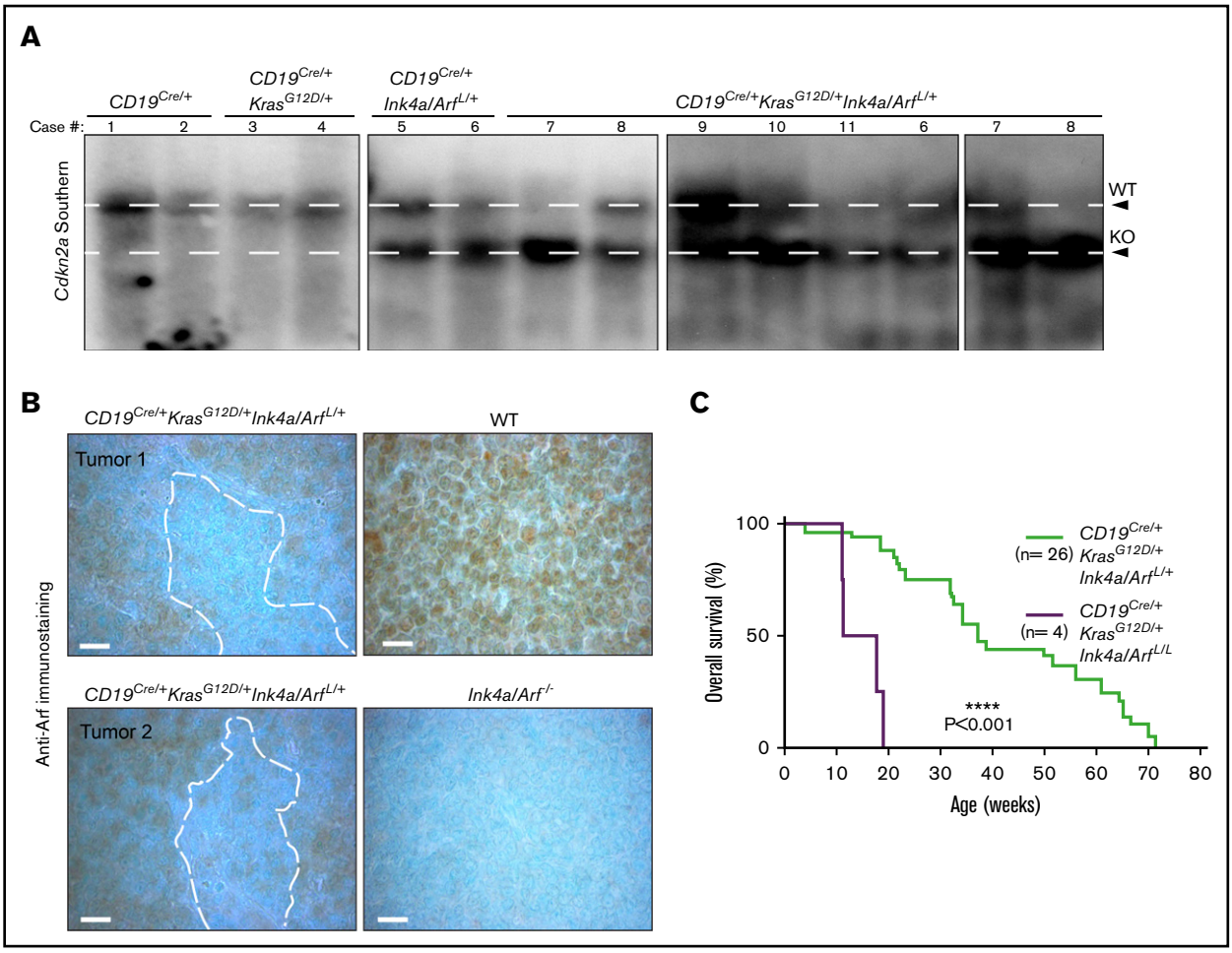

Figure 5. Loss of heterozygosity of the *Ink4a/Arf (Cdkn2a)* locus in pre-B-ALL. (A) Southern blot analysis of the *Ink4a/Arf* locus. WT, wild-type fragment of the *Ink4a/Arf* locus; KO, knockout configuration of the *Ink4a/Arf* locus. Loss of the upper WT band is indicative of loss of heterozygosity (LOH) of the *Ink4a/Arf* locus (see supplemental Figure 6). (B) Anti-Arf immunostains in the LNs of mice of the indicated genotypes. The specificity of Anti-Arf antibody was confirmed in LNs from *Ink4a/Arf*$^{-/-}$ mice. Scale bar, 10 μm. (C) Kaplan-Meier survival plot illustrating the impact of homozygous *Ink4a/Arf* deletion on survival of mice with Kras^{G12D} mutation in the B-cell compartment. *P* values were calculated by using the log-rank test.

Interestingly, RAS activation has been implicated in leukemogenesis in the myeloid compartment, promoting the development of indolent chronic myeloid leukemia (CML)[48] which in early stages before blast transformation, exhibits no alterations in the *INK4A/ARF* locus.[49] The transition of Ph+ CML to lymphoid blast crisis resembling pre-B-ALL is often accompanied by biallelic *INK4A/ARF* deletion.[50] Similarly, our finding that concerted Kras^{G12D} mutation and *Ink4a/Arf* deletion induce LOH at the WT *Ink4a/Arf* locus in mice without acquisition of universal secondary lesions before tumor development confirms that *Ink4a/Arf* is an important tumor suppressor of oncogenic Ras signaling in this in vivo model. Consistent with our findings, *Arf* inactivation in pre-B cells has been shown to augment BCR-ABL–induced development of B-ALL in transplantation models.[51,52] Although *Arf* was shown to be more important than *Ink4a* for B-ALL development,[51,52] we must presume that deletion of both proteins contributes to our phenotype because mice with *Ink4a* deletion were found to likewise develop high-grade B-cell malignancy.[53]

Acute oncogene activation is known to induce cellular stress resulting in senescence or apoptosis.[54] Kras-induced oncogenic stress in low-grade leukemia/lymphoma may not suffice by itself to activate cell-cycle checkpoints or might be accompanied by additional cooperating events (as in CML[48]) whose identification would necessitate larger cohorts of animals than the one used in this study. Nevertheless, loss of *Ink4a/Arf* (2 powerful tumor suppressors) presumably removes the cell-cycle control mechanisms restricting Kras^{G12D}-induced proliferation[23,49] and thus enhances B-ALL development. Our results suggest that additional regulatory mechanisms may well be at play. For instance, deletion of *Ink4a/Arf* in CD19^{+} B cells with Kras^{G12D} mutation not only suppresses oncogenic stress-related signatures such as DNA replication or oxidative stress[55] but also inhibits Kras^{G12D}-induced transcriptional profiles almost globally and reduces the number of proliferating cells. In line with these findings, it has been shown that activation of oncogenes such as BCR-ABL in pre-B cells induces apoptosis. Importantly, rare surviving cells acquired mutations in genes that negatively regulate ERK kinase activity, a downstream target of RAS/MAPK pathway,[56] which could point to attenuation of RAS activity as a necessary condition for induction of leukemogenesis, and which would be important to

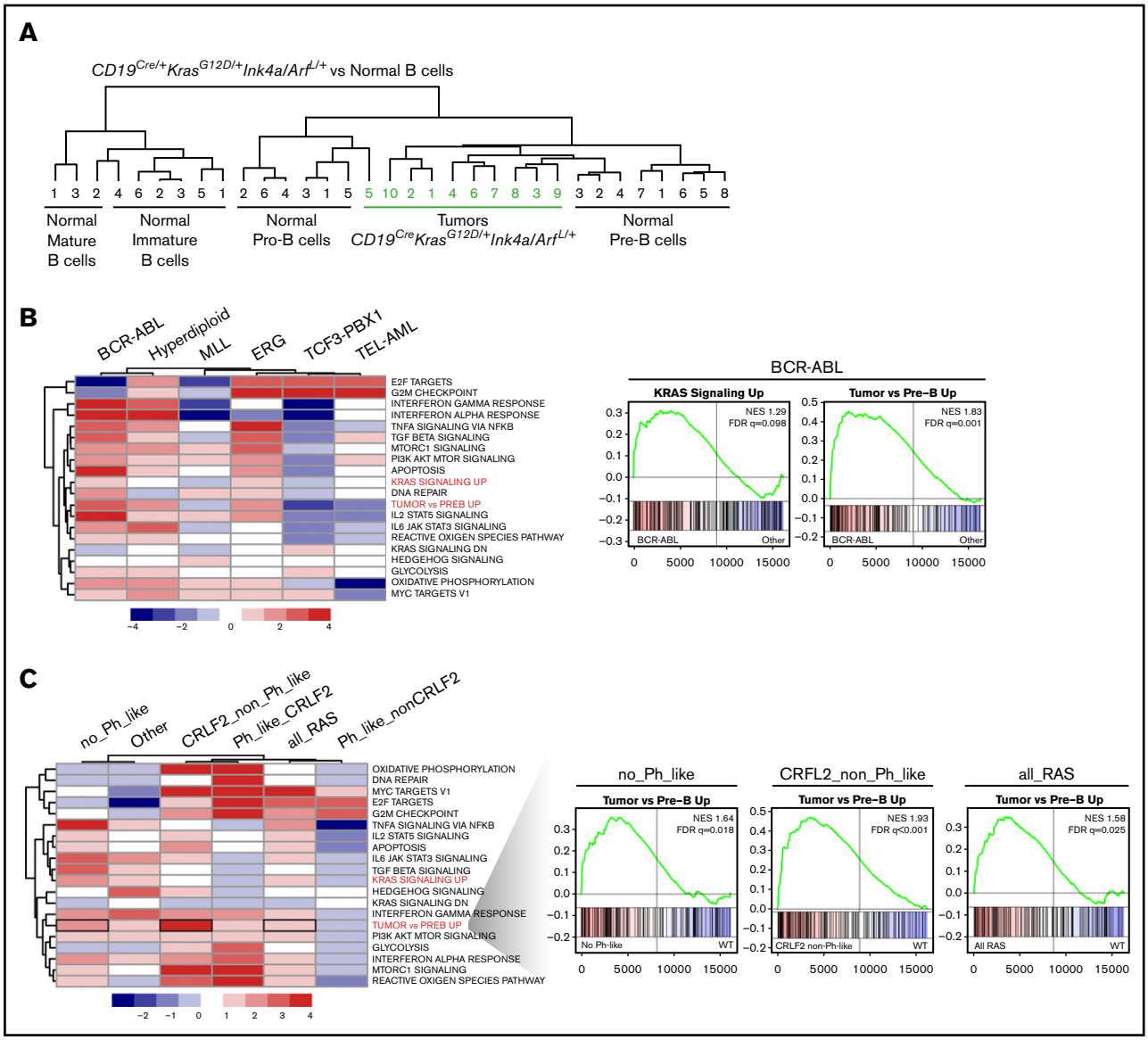

Figure 6. Pre-B-ALL arising in *CD19*$^{Cre/+}$ *Kras*$^{G12D/+}$ *Ink4a/Arf*$^{L/+}$ mice most closely resembles human BCR-ABL B-ALL. (A) Unsupervised hierarchical clustering of gene expression microarray profiles of B-ALL cells from *CD19*$^{Cre/+}$*Kras*$^{G12D/+}$*Ink4a/Arf*$^{L/+}$ mice and purified populations of normal mouse B cells at different stages of differentiation. (B) GSEA summary in indicated human B-ALL subtypes, each compared with all other samples. Color scale represents −log10 FDR from GSEA; positive sign reflects correlation to indicated subtype, negative to all other samples (left). Mountain plots illustrating upregulation of KRAS and our murine tumor signature in human B-ALL cells harboring *BCR-ABL* translocation (right). (C) GSEA summary in indicated human B-ALL subtypes with RAS mutations as indicated compared with samples with WT RAS. Samples from all RAS mutations combined (all_Ras), excluding patients classified as Ph-like (no_Phlike), only patients harboring *CRFL2* rearrangements with (Ph_like_CRLF2) or without Ph-like signature (CRLF2_non_Ph_like), or only patients classified as Ph-like without *CRFL2* rearrangements (Ph_like_nonCRLF2). Color scale represents −log10 FDR from GSEA; positive sign reflects correlation to samples with the indicated RAS mutations, negative to those with WT RAS (left). Mountain plots illustrating upregulation of murine tumor signature in human B-ALL cells within indicated group with KRAS mutations (right).

address when designing rational therapeutic strategies. Taken together, although these genomic changes may have different and in some way opposite effects, they nonetheless cooperate in the induction of B-ALL in vivo.

Although murine models of B-ALL already exist in the literature,[52,57-61] including transplantation models using BCR-ABL and mutated CRLF2 proteins as well as *Ink4a/Arf* knockouts, we believe that additional models of this disease are needed to more comprehensively encompass the molecular heterogeneity of B-ALL and to facilitate the study of oncogenic pathways potentially amenable to therapeutic intervention. Previous transgenic experimental models have probed the effects of *Ras* and/or *Ink4a/Arf* germ line alterations during hematopoiesis and have evaluated their potential for lymphomagenesis.[28,62] By using *CD19*-driven Cre recombinase, genomic alterations may be kept to the B-cell compartment, akin to somatic mutations in the human condition.

This does not affect the cells within the BM microenvironment and other hematopoietic elements which likely play an important role in leukemogenesis.[28,62] Few studies have yet created a murine model with which to predictively test new therapies specifically geared toward poor-prognosis and relapsed B-ALL.[52] Genome-wide expression analysis of human B-ALL at diagnosis/relapse has demonstrated the presence of significant alterations in multiple processes, such as cell-cycle regulation, proliferation, metabolism, DNA repair, signaling, and apoptosis[63,64] that are recapitulated in our *CD19*$^{Cre/+}$*Kras*$^{G12D/+}$*Ink4a/Arf*$^{L/+}$ mouse model. The short latency, full penetrance, activation of signaling pathways, and CD19 expression of our *CD19*$^{Cre/+}$*Kras*$^{G12D/+}$*Ink4a/Arf*$^{L/+}$ tumors in mice mimic the human setting and should facilitate future studies of kinase inhibitors as well as anti-CD19 chimeric antigen receptor T-cell therapies for pre-B-ALL.[65] We believe that our model represents an attractive alternative to existing syngeneic and xenograft models in terms of reflecting the human setting.

The clinical relevance of RAS and *INK4A/ARF* alterations at presentation are not conclusive and could be dependent on the B-ALL subtype.[41,66,67] However, the high incidence of their acquisition by leukemic cells during relapse suggests important roles in chemotherapy resistance and disease progression in humans.[9-13,19,68-71] Furthermore, the functional cooperation and the negative impact on survival of concurrent Ras mutation and *Ink/Arf* deletion in mice suggest that these changes may also have a functional impact in human B-ALL and should be considered in the course of disease classification, as well as for prognosis and choice of therapy in human subjects.

Acknowledgments

The authors thank Ronald DePinho for providing *Kras*$^{G12D/+}$ and *Ink4a/Arf*$^{L/+}$ mice and Klaus Rajewsky for providing the CD19^{Cre} mice.

This work was supported by National Institutes of Health (NIH), National Cancer Institute National Research Service Award F30 CA165857 (K.S.), by the Case Western Reserve Medical Scientist Training Program, by an NIH National Institute of General Medical Sciences grant (T32 GM007250), by a senior award from the Multiple Myeloma Research Foundation (R.D.C.), by Doctor's Cancer Foundation, and by NIH National Cancer Institute grants 1R01CA151391-01 and 1R01CA196783-01.

Authorship

Contribution: K.S., T.S., J.N.R., D.M.W., N.E.S., and R.D.C. designed the research; K.S., M.J., T.S., Y.K., A.A., R.L., Z.S., P.S.D., J.X., and M.E.L. performed the research; J.N.R., G.S.P., K.R., and C.G.M. contributed vital new agents or analytical tools; T.S., K.S., M.J., S.S.P., B.L., Y.Z., M.E.L., N.E.S., and R.D.C. analyzed data; and T.S., K.S., S.S.P., M.E.L., D.M.W., N.E.S., and R.D.C. wrote the paper.

Conflict-of-interest disclosure: The authors declare no competing financial interests.

Correspondence: Ruben D. Carrasco, Dana-Farber Cancer Institute, 450 Brookline Ave, JF215H, Boston, MA 02215; e-mail: ruben_carrasco@dfci.harvard.edu.

References

1. Swerdlow SH, Campo E, Harris NL, et al. *WHO Classification of Tumours of Haematopoietic and Lymphoid Tissues*. Lyon, France: IARC Press; 2008.
2. Raetz EA, Bhatla T. Where do we stand in the treatment of relapsed acute lymphoblastic leukemia? *Hematology Am Soc Hematol Educ Program*. 2012; 2012:129-136.
3. Stock W. Adolescents and young adults with acute lymphoblastic leukemia. *Hematology Am Soc Hematol Educ Program*. 2010;2010:21-29.
4. Collins-Underwood JR, Mullighan CG. Genomic profiling of high-risk acute lymphoblastic leukemia. *Leukemia*. 2010;24(10):1676-1685.
5. Roberts KG, Mullighan CG. Genomics in acute lymphoblastic leukaemia: insights and treatment implications. *Nat Rev Clin Oncol*. 2015;12(6):344-357.
6. Den Boer ML, van Slegtenhorst M, De Menezes RX, et al. A subtype of childhood acute lymphoblastic leukaemia with poor treatment outcome: a genome-wide classification study. *Lancet Oncol*. 2009;10(2):125-134.
7. Mullighan CG, Collins-Underwood JR, Phillips LA, et al. Rearrangement of CRLF2 in B-progenitor- and Down syndrome-associated acute lymphoblastic leukemia. *Nat Genet*. 2009;41(11):1243-1246.
8. Mullighan CG, Zhang J, Harvey RC, et al. JAK mutations in high-risk childhood acute lymphoblastic leukemia. *Proc Natl Acad Sci USA*. 2009;106(23): 9414-9418.
9. Knight T, Irving JA. Ras/Raf/MEK/ERK pathway activation in childhood acute lymphoblastic leukemia and its therapeutic targeting. *Front Oncol*. 2014;4: 160.
10. Irving JA. Towards an understanding of the biology and targeted treatment of paediatric relapsed acute lymphoblastic leukaemia. *Br J Haematol*. 2016; 172(5):655-666.
11. Mullighan CG, Zhang J, Kasper LH, et al. CREBBP mutations in relapsed acute lymphoblastic leukaemia. *Nature*. 2011;471(7337):235-239.
12. Irving J, Matheson E, Minto L, et al. Ras pathway mutations are prevalent in relapsed childhood acute lymphoblastic leukemia and confer sensitivity to MEK inhibition. *Blood*. 2014;124(23):3420-3430.
13. Davidsson J, Paulsson K, Lindgren D, et al. Relapsed childhood high hyperdiploid acute lymphoblastic leukemia: presence of preleukemic ancestral clones and the secondary nature of microdeletions and RTK-RAS mutations. *Leukemia*. 2010;24(5):924-931.
14. Mandanas RA, Leibowitz DS, Gharehbaghi K, et al. Role of p21 RAS in p210 bcr-abl transformation of murine myeloid cells. *Blood*. 1993;82(6): 1838-1847.
15. Pendergast AM, Quilliam LA, Cripe LD, et al. BCR-ABL-induced oncogenesis is mediated by direct interaction with the SH2 domain of the GRB-2 adaptor protein. *Cell*. 1993;75(1):175-185.

16. Yoda A, Yoda Y, Chiaretti S, et al. Functional screening identifies CRLF2 in precursor B-cell acute lymphoblastic leukemia. *Proc Natl Acad Sci USA*. 2010;107(1):252-257.

17. Takahashi-Tezuka M, Yoshida Y, Fukada T, et al. Gab1 acts as an adapter molecule linking the cytokine receptor gp130 to ERK mitogen-activated protein kinase. *Mol Cell Biol*. 1998;18(7):4109-4117.

18. Tasian SK, Doral MY, Borowitz MJ, et al. Aberrant STAT5 and PI3K/mTOR pathway signaling occurs in human CRLF2-rearranged B-precursor acute lymphoblastic leukemia. *Blood*. 2012;120(4):833-842.

19. Hogan LE, Meyer JA, Yang J, et al. Integrated genomic analysis of relapsed childhood acute lymphoblastic leukemia reveals therapeutic strategies. *Blood*. 2011;118(19):5218-5226.

20. Mullighan CG, Phillips LA, Su X, et al. Genomic analysis of the clonal origins of relapsed acute lymphoblastic leukemia. *Science*. 2008;322(5906):1377-1380.

21. Krentz S, Hof J, Mendioroz A, et al. Prognostic value of genetic alterations in children with first bone marrow relapse of childhood B-cell precursor acute lymphoblastic leukemia. *Leukemia*. 2013;27(2):295-304.

22. Quelle DE, Zindy F, Ashmun RA, Sherr CJ. Alternative reading frames of the INK4a tumor suppressor gene encode two unrelated proteins capable of inducing cell cycle arrest. *Cell*. 1995;83(6):993-1000.

23. Sherr CJ. The INK4a/ARF network in tumour suppression. *Nat Rev Mol Cell Biol*. 2001;2(10):731-737.

24. Mullighan CG, Miller CB, Radtke I, et al. BCR-ABL1 lymphoblastic leukaemia is characterized by the deletion of Ikaros. *Nature*. 2008;453(7191):110-114.

25. Roberts KG, Li Y, Payne-Turner D, et al. Targetable kinase-activating lesions in Ph-like acute lymphoblastic leukemia. *N Engl J Med*. 2014;371(11):1005-1015.

26. Rickert RC, Roes J, Rajewsky K. B lymphocyte-specific, Cre-mediated mutagenesis in mice. *Nucleic Acids Res*. 1997;25(6):1317-1318.

27. Tuveson DA, Shaw AT, Willis NA, et al. Endogenous oncogenic K-ras(G12D) stimulates proliferation and widespread neoplastic and developmental defects. *Cancer Cell*. 2004;5(4):375-387.

28. Serrano M, Lee H, Chin L, Cordon-Cardo C, Beach D, DePinho RA. Role of the INK4a locus in tumor suppression and cell mortality. *Cell*. 1996;85(1):27-37.

29. Jackson EL, Willis N, Mercer K, et al. Analysis of lung tumor initiation and progression using conditional expression of oncogenic K-ras. *Genes Dev*. 2001;15(24):3243-3248.

30. Aguirre AJ, Bardeesy N, Sinha M, et al. Activated Kras and Ink4a/Arf deficiency cooperate to produce metastatic pancreatic ductal adenocarcinoma. *Genes Dev*. 2003;17(24):3112-3126.

31. Carrasco DR, Fenton T, Sukhdeo K, et al. The PTEN and INK4A/ARF tumor suppressors maintain myelolymphoid homeostasis and cooperate to constrain histiocytic sarcoma development in humans. *Cancer Cell*. 2006;9(5):379-390.

32. Schindelin J, Arganda-Carreras I, Frise E, et al. Fiji: an open-source platform for biological-image analysis. *Nat Methods*. 2012;9(7):676-682.

33. Schindelin J, Rueden CT, Hiner MC, Eliceiri KW. The ImageJ ecosystem: an open platform for biomedical image analysis. *Mol Reprod Dev*. 2015;82(7-8):518-529.

34. Ruxton GD. The unequal variance t-test is an underused alternative to Student's t-test and the Mann-Whitney U test. *Behav Ecol*. 2006;17(4):688-690.

35. Carrasco DR, Tonon G, Huang Y, et al. High-resolution genomic profiles define distinct clinico-pathogenetic subgroups of multiple myeloma patients. *Cancer Cell*. 2006;9(4):313-325.

36. Cibulskis K, Lawrence MS, Carter SL, et al. Sensitive detection of somatic point mutations in impure and heterogeneous cancer samples. *Nat Biotechnol*. 2013;31(3):213-219.

37. Chin L, Pomerantz J, Polsky D, et al. Cooperative effects of INK4a and ras in melanoma susceptibility in vivo. *Genes Dev*. 1997;11(21):2822-2834.

38. Crews S, Barth R, Hood L, Prehn J, Calame K. Mouse c-myc oncogene is located on chromosome 15 and translocated to chromosome 12 in plasmacytomas. *Science*. 1982;218(4579):1319-1321.

39. Krivtsov AV, Feng Z, Lemieux ME, et al. H3K79 methylation profiles define murine and human MLL-AF4 leukemias. *Cancer Cell*. 2008;14(5):355-368.

40. Yeoh EJ, Ross ME, Shurtleff SA, et al. Classification, subtype discovery, and prediction of outcome in pediatric acute lymphoblastic leukemia by gene expression profiling. *Cancer Cell*. 2002;1(2):133-143.

41. Mullighan CG, Su X, Zhang J, et al; Children's Oncology Group. Deletion of IKZF1 and prognosis in acute lymphoblastic leukemia. *N Engl J Med*. 2009;360(5):470-480.

42. Ribeiro RC, Abromowitch M, Raimondi SC, Murphy SB, Behm F, Williams DL. Clinical and biologic hallmarks of the Philadelphia chromosome in childhood acute lymphoblastic leukemia. *Blood*. 1987;70(4):948-953.

43. Kang H, Chen IM, Wilson CS, et al. Gene expression classifiers for relapse-free survival and minimal residual disease improve risk classification and outcome prediction in pediatric B-precursor acute lymphoblastic leukemia. *Blood*. 2010;115(7):1394-1405.

44. Harvey RC, Mullighan CG, Wang X, et al. Identification of novel cluster groups in pediatric high-risk B-precursor acute lymphoblastic leukemia with gene expression profiling: correlation with genome-wide DNA copy number alterations, clinical characteristics, and outcome. *Blood*. 2010;116(23):4874-4884.

45. Case M, Matheson E, Minto L, et al. Mutation of genes affecting the RAS pathway is common in childhood acute lymphoblastic leukemia. *Cancer Res*. 2008;68(16):6803-6809.

46. Spina V, Khiabanian H, Messina M, et al. The genetics of nodal marginal zone lymphoma. *Blood*. 2016;128(10):1362-1373.

47. Treon SP, Xu L, Yang G, et al. MYD88 L265P somatic mutation in Waldenström's macroglobulinemia. *N Engl J Med*. 2012;367(9):826-833.

48. Wang J, Liu Y, Li Z, et al. Endogenous oncogenic Nras mutation promotes aberrant GM-CSF signaling in granulocytic/monocytic precursors in a murine model of chronic myelomonocytic leukemia. *Blood*. 2010;116(26):5991-6002.

49. Mullighan CG, Williams RT, Downing JR, Sherr CJ. Failure of CDKN2A/B (INK4A/B-ARF)-mediated tumor suppression and resistance to targeted therapy in acute lymphoblastic leukemia induced by BCR-ABL. *Genes Dev*. 2008;22(11):1411-1415.

50. Sill H, Goldman JM, Cross NC. Homozygous deletions of the p16 tumor-suppressor gene are associated with lymphoid transformation of chronic myeloid leukemia. *Blood*. 1995;85(8):2013-2016.

51. Signer RA, Montecino-Rodriguez E, Witte ON, Dorshkind K. Immature B-cell progenitors survive oncogenic stress and efficiently initiate Ph+ B-acute lymphoblastic leukemia. *Blood*. 2010;116(14):2522-2530.

52. Williams RT, Roussel MF, Sherr CJ. Arf gene loss enhances oncogenicity and limits imatinib response in mouse models of Bcr-Abl-induced acute lymphoblastic leukemia. *Proc Natl Acad Sci USA*. 2006;103(17):6688-6693.

53. Liu Y, Johnson SM, Fedoriw Y, et al. Expression of p16(INK4a) prevents cancer and promotes aging in lymphocytes. *Blood*. 2011;117(12):3257-3267.

54. Macheret M, Halazonetis TD. DNA replication stress as a hallmark of cancer. *Annu Rev Pathol*. 2015;10(1):425-448.

55. Maya-Mendoza A, Ostrakova J, Kosar M, et al. Myc and Ras oncogenes engage different energy metabolism programs and evoke distinct patterns of oxidative and DNA replication stress. *Mol Oncol*. 2015;9(3):601-616.

56. Shojaee S, Caeser R, Buchner M, et al. Erk negative feedback control enables Pre-B cell transformation and represents a therapeutic target in acute lymphoblastic leukemia. *Cancer Cell*. 2015;28(1):114-128.

57. Cook GJ, Pardee TS. Animal models of leukemia: any closer to the real thing? *Cancer Metastasis Rev*. 2013;32(1-2):63-76.

58. Jacoby E, Chien CD, Fry TJ. Murine models of acute leukemia: important tools in current pediatric leukemia research. *Front Oncol*. 2014;4:95.

59. Wu SC, Li LS, Kopp N, et al. Activity of the type II JAK2 inhibitor CHZ868 in B cell acute lymphoblastic leukemia. *Cancer Cell*. 2015;28(1):29-41.

60. Hauer J, Mullighan C, Morillon E, et al. Loss of p19Arf in a Rag1(-/-) B-cell precursor population initiates acute B-lymphoblastic leukemia. *Blood*. 2011; 118(3):544-553.

61. Wang PY, Young F, Chen CY, et al. The biologic properties of leukemias arising from BCR/ABL-mediated transformation vary as a function of developmental origin and activity of the p19ARF gene. *Blood*. 2008;112(10):4184-4192.

62. Tamai H, Miyake K, Takatori M, et al. Activated K-Ras protein accelerates human MLL/AF4-induced leukemo-lymphomogenicity in a transgenic mouse model. *Leukemia*. 2011;25(5):888-891.

63. Staal FJ, de Ridder D, Szczepanski T, et al. Genome-wide expression analysis of paired diagnosis-relapse samples in ALL indicates involvement of pathways related to DNA replication, cell cycle and DNA repair, independent of immune phenotype. *Leukemia*. 2010;24(3):491-499.

64. Bhojwani D, Kang H, Moskowitz NP, et al. Biologic pathways associated with relapse in childhood acute lymphoblastic leukemia: a Children's Oncology Group study. *Blood*. 2006;108(2):711-717.

65. Maude SL, Teachey DT, Porter DL, Grupp SA. CD19-targeted chimeric antigen receptor T-cell therapy for acute lymphoblastic leukemia. *Blood*. 2015; 125(26):4017-4023.

66. Perentesis JP, Bhatia S, Boyle E, et al. RAS oncogene mutations and outcome of therapy for childhood acute lymphoblastic leukemia. *Leukemia*. 2004; 18(4):685-692.

67. Carter TL, Watt PM, Kumar R, et al. Hemizygous p16(INK4A) deletion in pediatric acute lymphoblastic leukemia predicts independent risk of relapse. *Blood*. 2001;97(2):572-574.

68. Maloney KW, McGavran L, Odom LF, Hunger SP. Acquisition of p16(INK4A) and p15(INK4B) gene abnormalities between initial diagnosis and relapse in children with acute lymphoblastic leukemia. *Blood*. 1999;93(7):2380-2385.

69. Carter TL, Reaman GH, Kees UR. INK4A/ARF deletions are acquired at relapse in childhood acute lymphoblastic leukaemia: a paired study on 25 patients using real-time polymerase chain reaction. *Br J Haematol*. 2001;113(2):323-328.

70. Polak A, Kiliszek P, Sewastianik T, et al. MEK inhibition sensitizes precursor B-cell acute lymphoblastic leukemia (B-ALL) cells to dexamethasone through modulation of mTOR activity and stimulation of autophagy. *PLoS One*. 2016;11(5):e0155893.

71. Garza AS, Miller AL, Johnson BH, Thompson EB. Converting cell lines representing hematological malignancies from glucocorticoid-resistant to glucocorticoid-sensitive: signaling pathway interactions. *Leuk Res*. 2009;33(5):717-727.